Multiphase Region-based Active Contours for Semi-automatic Segmentation of Brain MRI Images

Farhan Akram[1], Domenec Puig[1], Miguel Angel Garcia[2] and Adel Saleh[1]
[1]*Department of Computer Engineering and Mathematics, Rovira i Virgili University, 43007 Tarragona, Spain*
[2]*Department of Electronic and Communications Technology, Autonomous University of Madrid, 28049 Madrid, Spain*

Keywords: Active Contours, Medical Image Analysis, Segmentation, Thresholding.

Abstract: Segmenting brain magnetic resonance (MRI) images of the brain into white matter (WM), grey matter (GM) and cerebrospinal fluid (CSF) is an important problem in medical image analysis. The study of these regions can be useful for determining different brain disorders, assisting brain surgery, post-surgical analysis, saliency detection and for studying regions of interest. This paper presents a segmentation method that partitions a given brain MRI image into WM, GM and CSF regions through a multiphase region-based active contour method followed by a pixel correction thresholding stage. The proposed region-based active contour method is applied in order to partition the input image into four different regions. Three of those regions within the brain area are then chosen by intersecting a hand-drawn binary mask with the computed contours. Finally, an efficient thresholding-based pixel correction method is applied to the computed WM, GM and CSF regions to increase their accuracy. The segmentation results are compared with ground truths to show the performance of the proposed method.

1 INTRODUCTION

Image segmentation is a basic yet necessary task for many medical applications, such as surgical planning, post-surgical analysis, saliency detection and study of regions of interest (Zhang et al., 2007). Segmentation of brain MRI images is a well-known problem in medical image analysis. Its goal is to segment the brain area into different disjoint regions: grey matter (GM), white matter (WM) and cerebrospinal fluid (CSF). Due to the geometric complexity of the human brain cortex, manual slice-by-slice segmentation is cumbersome and time consuming. The complexity of intensity inhomogeneous regions makes brain MRI images hard to segment with high accuracy (Balafar et al., 2010). Numerous methods have been devised to segment the brain into different non-overlapping regions (Elnakib et al., 2011). In particular, the active contour method introduced in (Kass et al., 1988) is widely-used for image segmentation. In this method, a curve evolves towards the boundaries of the object of interest under a certain force field by minimizing the curve's intrinsic energy.

Active contour models can be classified into two main categories: edge-based (Kass et al., 1988; Caselles et al., 1997; Li et al., 2005) and region-based (Mumford and Shah, 1989; Chan and Vese, 2001; Li et al., 2007; Li et al., 2008; Zhang et al., 2010; Akram et al., 2013; Akram et al., 2014) methods. Edge-based active contour methods, which use an edge-indicator function to drive the contour towards the object boundaries, can hardly stop the evolution of the contour with weak or blurred edges. Alternatively, region-based active contour methods, which use image statistical information, can properly segment the image even with such weak or blurred edges. However, the traditional active contour method (Mumford and Shah, 1989; Chan and Vese, 2001) is defined under the assumption that the target image is homogeneous. Therefore, it cannot properly segment images with intensity inhomogeneous regions. Although both edge-based and region-based active contour methods have their own pros and cons, region-based methods usually perform better than edge-based methods (Zhang et al., 2010; Yang et al., 2010).

In (Vese and Chan, 2002), a multiphase level set framework using n level sets was proposed to segment a given image into 2^n phases (regions). This method is the extension to multiphase level sets of a previous work on active contours without edges (Chan and Vese, 2001). It was developed under the assumption that the input image must have homogeneous inten-

Akram F., Puig D., Garcia M. and Saleh A..
Multiphase Region-based Active Contours for Semi-automatic Segmentation of Brain MRI Images.
DOI: 10.5220/0005294804470454
In *Proceedings of the 10th International Conference on Computer Vision Theory and Applications* (VISAPP-2015), pages 447-454
ISBN: 978-989-758-089-5

sity regions. Therefore, it does not properly work on images that contain inhomogeneous regions or with small intensity differences among different regions.

In (Li et al., 2007; Li et al., 2008), a region-based active contour method was proposed in the context of intensity inhomogeneous regions. It computes the image intensity mean over a local neighbourhood by using a Gaussian kernel. Although that method can successfully segment images with intensity inhomogeneity, it has a significantly high computational complexity. Moreover, segmentation results of different regions can overlap if the objects in the image have a complex geometry.

In (Zhang et al., 2010), a region-based active contour method was proposed based on a local fitted image generated by using the local mean values proposed in (Li et al., 2007; Li et al., 2008). This method is also able to segment images with inhomogeneous intensity regions, although it is less accurate than the latter and also suffers from the region overlapping problem in case of complex geometries such as brain regions. Alternatively, a region-based active contour method for brain MRI image segmentation was proposed in (Akram et al., 2013; Akram et al., 2014). That method applies a locally-computed active contour method based on a signed pressure force (SPF) function in order to segment the brain into WM and GM regions. It has a lower computational complexity and yields better segmentation results than the aforementioned methods. However, since it is a two-phase active contour method, it can only segment the input images into two disjoint regions.

In the present paper, a four-phase region-based active contour method is proposed. It applies two-phase local and global fitted image models in order to define a four-phase active contour energy functional. The proposed method aims to segment the brain area from a brain MRI image into three different non-overlapping regions: WM, GM and CSF. This method consists of three stages. In the first stage, a new four-phase region-based active contour method is applied to yield an initial segmentation of the given brain MRI image. In the next stage, a hand-drawn binary mask of the brain area is intersected with the final contours obtained in the previous stage in order to constrain the contour evolution to the brain area. In the last stage, a thresholding-based pixel correction method is finally applied in order to improve the segmentation results of WM, GM and CSF regions. Experimental results show that the proposed method yields segmentation accuracies of around 91% for WM regions, 87% for GM and 80% for CSF regions.

This paper is organized as follows. The three stages of the proposed method are described in section 2. Experimental results are shown in section 3. Finally, conclusions and further research lines are given in section 4.

2 SEGMENTATION OF REGIONS OF INTEREST IN MRI BRAIN IMAGES

The proposed method to segment regions of interest in MRI brain images consists of three stages described below. The first stage segments the regions of interest using a new region-based active contour method. The second stage constrains the level set functions defined in the previous stage by intersecting their contours with a hand-drawn binary mask of the brain area. The third stage performs a thresholding-based pixel correction of the computed WM, GM and CSF regions.

2.1 Multiphase Region-based Active Contours

Since a piecewise active contour model based on a two-phase level set function (Chan and Vese, 2001) is able to segment a given image into two distinct regions, it cannot be applied to the segmentation of the three main regions of interest in the brain (WM, GM and CSF). Therefore, it is necessary to apply a four-phase level set method.

Active contours are dynamic curves that move toward the object boundaries to partition an image into distinct and non-overlapping regions. To segment a brain image into three non-overlapping regions, an energy functional is defined with both a region-based area term and an edge-based length term. With piecewise multiphase active contour methods, two level sets are necessary for segmenting an image into four distinct regions (Vese and Chan, 2002). The proposed energy functional utilizes the local and global mean intensity values of two level sets (Chan and Vese, 2001; Li et al., 2007; Li et al., 2008). Let $I\colon \Omega \rightarrow \mathbf{R}$ be an input image, $\Phi(\phi_1,\phi_2)$ be two level sets and $C(C_1,C_2)$ be the closed curves defined by the zero level sets corresponding to Φ. An energy functional $E(\Phi(\phi_1,\phi_2))$ is defined as follows:

$$E(\Phi(\phi_1,\phi_2)) = \lambda_1 F_{local}(\phi_1) + \lambda_2 F_{global}(\phi_2) + v_1 L_g(\phi_1) + v_2 L_g(\phi_2), \quad (1)$$

where $\lambda_1 > 0$, $\lambda_2 > 0$, v_1 and v_2 are constants, $L_g(\phi_1)$ and $L_g(\phi_2)$ are regularization terms that drive the zero level curves $C(C_1,C_2)$ into smooth curves by taking into account image edges, and $F_{local}(\phi_1)$ and $F_{global}(\phi_2)$ are force terms that use local and global

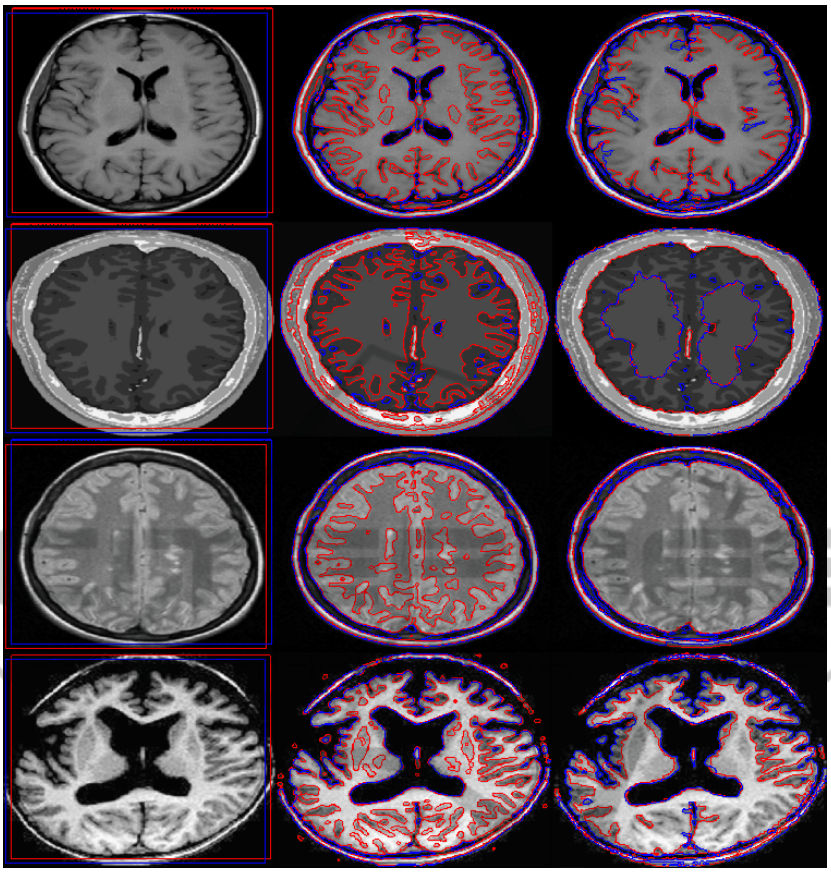

Figure 1: Brain MRI image segmentation comparison. The first column shows brain MRI images with initial contours. The second column shows the final contours using the proposed method. The third column shows the final contours using the multiphase level set framework proposed in (Vese and Chan, 2002).

fitted images defined by utilizing local and global intensity mean values as proposed in (Li et al., 2007; Li et al., 2008; Chan and Vese, 2001), respectively. The local force term $F_{local}(\phi_1)$ is based on mean values computed over a square neighbourhood and drives the first level set to weak and blurred edges by distinguishing inhomogeneous regions. In turn, the global force term $F_{global}(\phi_2)$ extracts the boundaries of dark homogeneous regions. By substituting $F_{local}(\phi_1)$, $F_{global}(\phi_2)$, $L_g(\phi_1)$ and $L_g(\phi_2)$ by their corresponding expressions (Li et al., 2005; Zhang et al., 2010), the following formulation is obtained:

$$\begin{aligned} E(\Phi(\phi_1,\phi_2)) = \lambda_1 &\int_\Omega |I(x) - I_{local}(x)|^2 dx \\ +\lambda_2 &\int_\Omega |I(x) - I_{global}(x)|^2 dx \\ +\nu_1 &\int_\Omega g(I)\delta_\varepsilon(\phi_1)|\nabla\phi_1| dx \\ +\nu_2 &\int_\Omega g(I)\delta_\varepsilon(\phi_2)|\nabla\phi_2| dx, \end{aligned} \quad (2)$$

where $\delta_\varepsilon(z) = \frac{\varepsilon}{\pi(z^2+\varepsilon^2)}$ is the regularized Dirac function, $H_\varepsilon(z) = \frac{1}{2}\left(1 + (\frac{2}{\pi})arctan(\frac{z}{\varepsilon})\right)$ is the regularized Heaviside function, and $g(I) = \frac{1}{1+|\nabla G_{\sigma_1} * I(x)|^2}$ is a positive and strictly decreasing edge indicator function. In turn, functions I_{local} and I_{global} are local and global fitted images respectively defined as:

$$I_{local} = f_1 H_\varepsilon(\phi_1) + f_2(1 - H_\varepsilon(\phi_1)) \quad (3)$$

$$I_{global} = c_1 H_\varepsilon(\phi_2) - c_2(1 - H_\varepsilon(\phi_2)), \quad (4)$$

In (3), f_1 and f_2 are the local mean values inside and outside of the object boundaries in the image, which are borrowed from (Li et al., 2007; Li et al., 2008) and defined as:

$$f_1 = \frac{K_{\sigma_1} * [H_\varepsilon(\phi_1) I(x)]}{K_{\sigma_1} * H_\varepsilon(\phi_1)} \quad (5)$$

$$f_2 = \frac{K_{\sigma_1} * [(1 - H_\varepsilon(\phi_1)) I(x)]}{K_{\sigma_1} * (1 - H_\varepsilon(\phi_1))}, \quad (6)$$

where σ_1 is the standard deviation of the truncated Gaussian kernel, which is used to compute the local

intensity means of the image. In (4), c_1 and c_2 are the global mean values inside and outside of the object boundaries in the image, which are borrowed from (Chan and Vese, 2001) and defined as:

$$c_1 = \frac{\int_\Omega H_\varepsilon(\phi_2) I(x) dx}{\int_\Omega H_\varepsilon(\phi_2) dx} \tag{7}$$

$$c_2 = \frac{\int_\Omega (1 - H_\varepsilon(\phi_2)) I(x) dx}{\int_\Omega (1 - H_\varepsilon(\phi_2)) dx}, \tag{8}$$

By differentiating (2) using the calculus of variations (Aubert and Kornprobst, 2006), the partial derivatives of functional $E(\Phi(\phi_1, \phi_2))$ can be written as:

$$\frac{\partial \phi_1}{\partial t} = \lambda_1 (I(x) - I_{local})(f_1 - f_2)\delta_\varepsilon(\phi_1) + v_1 div\left(g(I)\frac{\nabla \phi_1}{|\nabla \phi_1|}\right)\delta_\varepsilon(\phi_1) \tag{9}$$

$$\frac{\partial \phi_2}{\partial t} = \lambda_2 (I(x) - I_{global})(c_2 - c_1)\delta_\varepsilon(\phi_2) + v_2 div\left(g(I)\frac{\nabla \phi_2}{|\nabla \phi_2|}\right)\delta_\varepsilon(\phi_2), \tag{10}$$

The function $\Phi(\phi_1, \phi_2)$ that minimizes the energy functional $E(\Phi(\phi_1, \phi_2))$ in (2) satisfies the Euler Lagrange equation $-\frac{\partial E(\Phi)}{\partial \phi_1} = 0$ and $-\frac{\partial E(\Phi)}{\partial \phi_2} = 0$. In (9) and (10), $\lambda_1(f_1 - f_2))$ and $\lambda_2(c_2 - c_1))$ can respectively be replaced by constants γ_1 and γ_2:

$$\frac{\partial \phi_1}{\partial t} = \gamma_1 (I(x) - I_{local})\delta_\varepsilon(\phi_1) + v_1 div\left(g(I)\frac{\nabla \phi_1}{|\nabla \phi_1|}\right)\delta_\varepsilon(\phi_1) \tag{11}$$

$$\frac{\partial \phi_2}{\partial t} = \gamma_2 (I(x) - I_{global})\delta_\varepsilon(\phi_2) + v_2 div\left(g(I)\frac{\nabla \phi_2}{|\nabla \phi_2|}\right)\delta_\varepsilon(\phi_2), \tag{12}$$

A signed distance function (SDF) defined below is used for the initialization of the level set functions:

$$\phi_i(x,t) = \begin{cases} -\rho, & x \in \Omega - O_i \\ 0, & x \in \partial O_i \\ \rho, & x \in O_i, \end{cases} \tag{13}$$

where $\rho > 0$ is a constant ($\rho = 1$ in this work). In (11), $t = 0$ and $i = 1,2$ define the initial conditions of both level set functions. After evolving the level set functions using (9) and (10), they are regularized by using $\phi_i^k = G_{\sigma_2} * \phi_i^k$, where $i = 1,2$ represents the number of level sets and k is the iteration number during the curve evolution. The regularization mentioned above not only regularizes the level set functions but also eliminates the need for re-initialization, which is computationally very expensive. Here, σ_2 is the standard deviation of the Gaussian kernel used in the regularization process.

Figure 1 shows a visual comparison of the proposed method against the multiphase level set method proposed in (Vese and Chan, 2002). This result shows that the latter cannot properly segment the given images, since the intensity average obtained in that four-phase active contour method is computed globally over the whole image. Therefore, it cannot distinguish between different intensity levels if the intensity differences are too small.

However, the proposed method, which utilizes intensity means computed both locally and globally over the image, can successfully segment non-overlapping regions. Local intensity means are used to distinguish small intensity differences and to segment intensity inhomogeneous regions, whereas global intensity means are used to segment dark homogeneous regions. By using local intensity means for small intensity difference, which may refers to weak edges and incorporating global means for sharp edges, the proposed method also deals with the energy leakage problem. For the local computation of intensity means, the proposed method applies the Gaussian kernel defined in (Li et al., 2007; Li et al., 2008), which is able to distinguish small intensity differences in a local neighbourhood. Therefore, it can properly segment small regions in the image.

2.2 Extraction of WM, GM and CSF Regions

In this stage, the brain region is first delimited by using a binary mask manually defined by drawing the contour along the boundary of the brain area. After generating that mask, the level sets corresponding to the final contours inside the brain area are extracted by intersecting each level set obtained in the previous stage with the new binary mask. The combination of these modified level sets is then used to define the WM, GM and CSF regions as follows. Let $\phi_i(x,y)$ be the level sets associated with a given brain MRI image $I(x,y)$, $i = 1,2$, be the number of level set and $mask(x,y)$ be the hand-drawn binary mask of the brain area. The modified level sets $\zeta_i(x,y)$ restricted to the brain area can be described as:

$$\zeta_i(x,y) = \phi_i(x,y) \cap mask(x,y), \tag{14}$$

The combination of modified level sets that yields

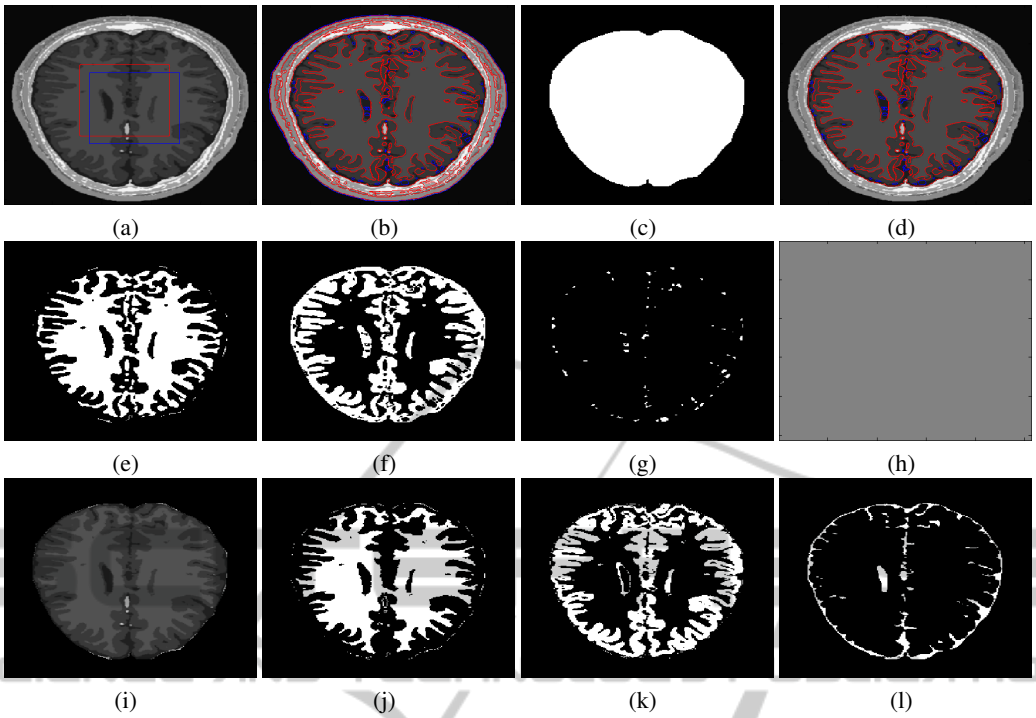

Figure 2: Stages of the proposed algorithm. (a) Initial contour, (b) final contour, (c) binary mask of the brain region, (d) final contour restricted to brain area, (e) $\zeta_1 > 0$ and $\zeta_2 > 0$ WM region, (f) $\zeta_1 < 0$ and $\zeta_2 > 0$ GM region, (g) $\zeta_1 < 0$ and $\zeta_2 < 0$ CSF region, (h) $\zeta_1 > 0$ and $\zeta_2 < 0$ region (empty or zero region, which is discarded), (i) extracted brain region with the binary mask, (j) final WM region, (k) final GM region, (l) final CSF region.

the WM, GM and CSF binary regions is then defined as:

$$WM(x,y) = (\zeta_1(x,y) > 0) \cap (\zeta_2(x,y) > 0),$$

$$GM(x,y) = (\zeta_1(x,y) < 0) \cap (\zeta_2(x,y) > 0),$$

$$CSF(x,y) = (\zeta_1(x,y) < 0) \cap (\zeta_2(x,y) < 0),$$

Figures 2 (e), (f) and (g), respectively show an example of the WM, GM and CSF regions computed with the above combination of modified level set functions.

2.3 Pixel Correction

In this last stage, the segmentation results obtained after the previous stage are modified according to a pixel correction algorithm based on simple thresholding. The WM, GM and CSF binary regions computed in previous stage are intersected with the input grey-level image to compute the intensity average of their non-zero pixels. These averages are then used to define a set of thresholds. If N is the number of rows and columns ($N = 256$ in this work), the intensity means corresponding to the three regions of interest are respectively defined as:

$$\overline{WM}(x,y) = \frac{\sum_{x=1}^{N}\sum_{y=1}^{N} I(x,y)WM(x,y)}{\sum_{x=1}^{N}\sum_{y=1}^{N} WM(x,y)} \quad (15)$$

$$\overline{GM}(x,y) = \frac{\sum_{x=1}^{N}\sum_{y=1}^{N} I(x,y)GM(x,y)}{\sum_{x=1}^{N}\sum_{y=1}^{N} GM(x,y)} \quad (16)$$

$$\overline{CSF}(x,y) = \frac{\sum_{x=1}^{N}\sum_{y=1}^{N} I(x,y)CSF(x,y)}{\sum_{x=1}^{N}\sum_{y=1}^{N} CSF(x,y)}, \quad (17)$$

The binary images corresponding to the regions of interest are finally defined as:

$$WM(x,y) = \begin{cases} 1, & \frac{\overline{WM}}{2} + 128 > I(x,y) \geqslant \frac{\overline{WM}+\overline{GM}}{2} \\ 0, & otherwise \end{cases} \quad (18)$$

$$GM(x,y) = \begin{cases} 1, & \frac{\overline{GM}+\overline{WM}}{2} > I(x,y) \geqslant \frac{\overline{GM}+\overline{CSF}}{2} \\ 0, & otherwise \end{cases} \quad (19)$$

$$CSF(x,y) = \begin{cases} 1, & \frac{\overline{CSF}+\overline{GM}}{2} > I(x,y) \geqslant \frac{\overline{CSF}}{2} \\ 0, & otherwise \end{cases} \quad (20)$$

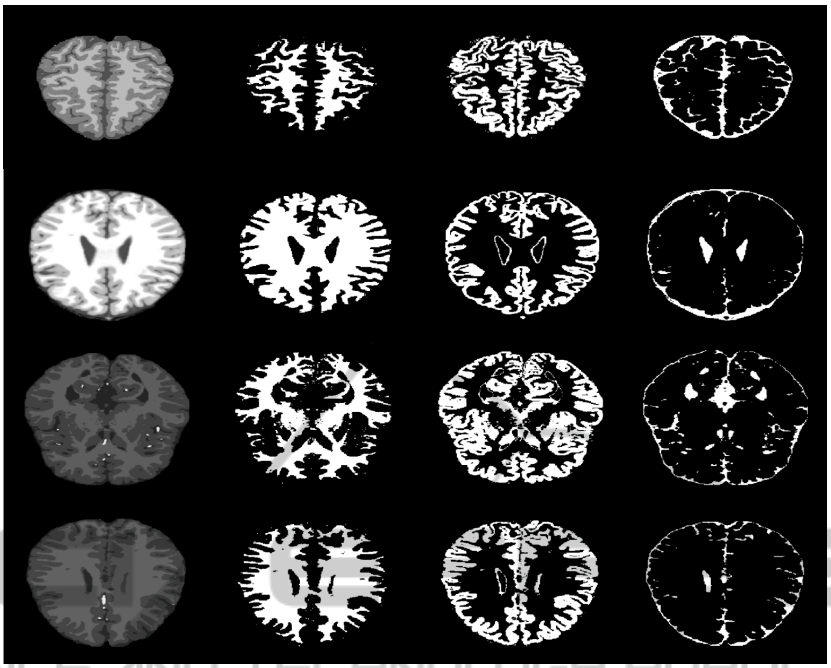

Figure 3: Segmentation of brain MRI image into distinct regions of interest. The first column shows the brain region after applying the brain mask. The second column shows the segmented WM region after pixel correction. The third column shows the segmented GM region after pixel correction. The fourth column shows the segmented CSF region after pixel correction.

3 EXPERIMENTAL RESULTS

The proposed method has been implemented using MATLAB 7.12 on a 3.4 GHz Intel Core-i7 with 16GB of RAM and tested on real brain MRI images of 256×256 pixels with 256 grey levels (8 bpp). These images correspond to 20 brain anatomical models (Brain, 2013). The following parameters have experimentally been chosen: $v_1 = 1$, $v_2 = 1$, $\gamma_1 = 1.5$, $\gamma_2 = 1$, $\varepsilon = 1.5$, $\rho = 1$, $\sigma_1 = 3$, $\sigma_2 = 1$, time step $\tau = 1$, and number of iterations $n = 200$.

Figure 2 shows results of the three stages of the proposed method. Figure 2(a) shows a brain MRI image with the initial contour. Figure 2(b) shows the final contour using the proposed four-phase active contour method. Figure 2(c) shows the hand-drawn binary mask of the brain area. Figure 2(d) displays the final contour after restricting the growth of the level set function to the brain area. Figure 2(e) shows the extracted WM region from the modified level set function with $\zeta_1 > 0$ and $\zeta_2 > 0$. Figure 2(f) shows the extracted GM region obtained from the combination of the modified level set with $\zeta_1 < 0$ and $\zeta_2 > 0$. Figure 2(g) shows the extracted CSF region obtained from the modified level set function with $\zeta_1 < 0$ and $\zeta_2 < 0$. Figure 2(h) shows the zero region obtained from the modified level set function with $\zeta_1 > 0$ and $\zeta_2 < 0$. Figure 2(i) shows the segmented brain region by intersecting the given brain MRI image with the binary mask of the brain region shown in Figure 2(c). Figure 2(j) displays the final WM region after applying the pixel correction algorithm on the WM region in Figure 2(e). Figure 2(k) displays the final GM region after applying the pixel correction algorithm on the GM region in Figure 2(f). Finally, Figure 2(l) displays the final CSF region after applying the pixel correction algorithm on the CSF region in Figure 2(g).

Table 1: Percentage accuracy for test subject 035.

Slice number	WM accuracy%	GM accuracy%	CSF accuracy%
100	83.64	90.85	78.74
120	92.63	91.45	75.13
140	95.21	91.61	76.97
160	93.99	91.01	78.97
180	95.12	90.24	80.53
200	96.58	92.33	76.50
220	95.96	92.62	77.99
240	93.17	89.73	80.29
250	91.69	87.45	83.08
260	91.23	85.80	82.69
280	85.40	77.93	84.60
300	75.32	67.53	83.22

Table 2: Percentage accuracy of Vese-Chan multiphase and proposed method after stage 2 and stage 3 using slice number 210 in all of the test data (Brain, 2013).

Test data	% Accuracy after stage 2						% Accuracy after stage 3					
	Vese-Chan method			Proposed method			Vese-Chan method			Proposed method		
	CSF	GM	WM	CSF	GM	WM	CSF	GM	WM	CSF	GM	WM
04	5.57	0.21	0.23	11.32	78.28	92.77	17.74	1.97	0.05	76.99	93.51	95.88
05	10.16	6.07	0.67	9.54	74.28	89.99	19.36	5.69	90.28	76.89	94.14	96.29
06	2.37	34.79	3.90	11.62	83.29	93.88	0.37	0	96.22	74.15	94.21	96.07
18	10.01	7.16	0.52	16.41	80.27	93.05	16.39	7.11	93.49	79.39	94.19	96.61
20	10.24	0	0	9.56	75.60	90.80	66.21	93.36	96.64	76.50	94.01	96.89
38	21.59	0.04	0.12	14.85	69.30	88.11	75.87	86.06	89.17	80.20	93.02	96.43
41	11.07	4.10	0.35	13.78	76.85	91.45	18.33	7.31	91.22	77.74	94.32	96.76
42	3.32	2.81	0.27	14.26	78.42	92.30	16.60	1.56	0.83	79.23	94.98	96.20
43	15.93	9.43	0.39	11.11	78.99	92.50	16.86	7.39	90.20	79.50	94.38	96.63
44	8.22	6.17	0.35	11.35	72.28	91.34	21.94	5.19	89.42	79.99	92.91	96.67
45	24.89	4.21	0.38	16.12	75.32	92.69	22.15	4.12	0.73	77.78	93.72	96.79
46	24.97	10.90	0.34	17.54	72.55	91	25.39	6.39	0.92	80.65	92.43	96.53
47	8.66	6.23	0.41	22.09	75.92	91.65	21.84	3.35	0	79.17	93.05	95.86
48	26.74	10.81	0.48	14.83	66.34	86.22	28.21	10.51	1.19	79.77	90.20	95.67
49	13.19	6.45	0.29	24.77	76.62	91.31	20.35	7.54	86.51	80.08	92.16	96.33
50	9.81	9.46	0.37	31.14	77.90	91.18	19.15	5.26	92.40	80.28	93.48	96.18
51	25.28	0	0	23.37	77.46	91.44	85.02	93.13	91.97	80.71	94.11	96.24
52	7.83	0	0	7.23	76.13	90.78	18.66	7.04	87.19	76.21	96.63	96.09
53	16.62	6.44	0.59	18.79	79.36	91.15	16.61	9.28	89.86	76.68	94.21	96.36
54	17.65	10.03	0.56	18.75	69.25	87.89	26.83	9.44	7.35	80.21	93.72	96.91

Table 1 shows the percentage accuracy of the segmentation results of WM, GM and CSF regions by comparing them with their respective ground truths. It displays the segmentation accuracy for different slices (2D images) of the test subject 04 from the 20 brain anatomical models (Brain, 2013). The percentage accuracy of the proposed method is computed by the following expression:

$$Accuracy = \frac{|A \cap B|}{|A \cup B|} \times 100,$$

where $|X|$ is the number of pixels equal to 1 (logical true) in a given binary image X, A is the binary image associated with the obtained region of interest (WM, GM or CSF) and B is the ground truth corresponding to that region.

Figure 3 shows the segmentation result of WM, GM and CSF regions using the proposed method. The first column in the figure displays the segmented brain area after intersecting the given brain MRI image with the hand-drawn binary mask of the brain region. The second column displays the segmented WM region after pixel correction. The third column displays the segmented GM region after pixel correction. Finally, the fourth column displays the segmented CSF region after pixel correction.

Table 2 shows, accuracy comparison of segmentation results between Vese-Chan and proposed methods with respect to given ground truth after stage 2 and stage 3. After stage 2, Vese-Chan method provides accuracy of 13.71%, 6.77% and 0.51% for CSF, GM and WM, respectively. After stage 3, Vese-Chan method provides accuracy of 27.69%, 18.59% and 59.78% for CSF, GM and WM, respectively. After stage 2, proposed method provides accuracy of 15.92%, 75.72% and 91.08% for CSF, GM and WM, respectively. After stage 3, proposed method provides accuracy of 78.61%, 93.67% and 96.37% for CSF, GM and WM, respectively.

Vese-Chan method that uses global intensity means cannot properly segment images with intensity inhomogeneity; therefore, it provides very less accuracy after stage 2. As we know that intensity inhomogeneous regions are not properly segmented by Vese-Chan method, therefore, pixel correction method in stage 3 cannot effectively improve its segmentation results.

The proposed method provides quite acceptable segmentation accuracy of GM and WM regions after stage 2. But it provides very less segmentation accuracy of CSF region. After applying pixel correction algorithm in stage 3 not only segmentation result of CSF is improved but also segmentation result of GM and WM are refined.

4 CONCLUSIONS AND FUTURE WORK

Segmentation of brain MRI images into distinct and non-overlapping regions, such as WM, GM and CSF, is a challenging problem due to the geometric complexity of the regions to be segmented. The presence of noise and intensity inhomogeneity in the image significantly increases the complexity of the problem. Since, there are three important regions (WM, GM and CSF) in the brain area, a four-phase level set method is necessary for segmenting the image into three or four regions. This paper presents a four-phase region based active contour method that segments an MRI brain image into WM, GM and CSF regions with a good accuracy. It uses both local and global intensity averages in the definition of an energy functional, such that local intensity mean values help the proposed model to segment regions with intensity inhomogeneity, whereas global intensity mean values are responsible for segmenting the homogeneous areas in the image. In addition, a pixel correction method based on simple thresholding is applied in order to correct wrong pixels.

As a future work we aim at developing a new energy functional that will be able to segment noisy intensity inhomogeneous images efficiently. This involves the definition of a more efficient and robust active contour method based on local texture regions. Another research goal is the development of an automatic technique to extract the brain area necessary for intersecting the obtained level sets, thus avoiding the hand-drawn binary mask utilized in the second stage of the proposed technique.

ACKNOWLEDGEMENTS

This work was supported by the Spanish Government through project TIN2012-37171-C02-02 and Catalan Government Predoctoral grant AGAUR FI-DGR 2014.

REFERENCES

Akram, F., Kim, J. H., and Choi, K. N. (2013). Active contour method with locally computed signed pressure force function: An application to brain mr image segmentation. In *Seventh International Conference on Image and Graphics (ICIG)*, pages 154–159. IEEE.

Akram, F., Kim, J. H., Lim, H. U., and Choi, K. N. (2014). Segmentation of intensity inhomogeneous brain mr images using active contours. *Computational and Mathematical Methods in Medicine*, 2014:1–14.

Aubert, G. and Kornprobst, P. (2006). *Mathematical Problems in Image Processing: Partial Differential Equations and the Calculus of Variations*. Springer, New York, 2nd edition.

Balafar, M. A., Ramli, A. R., Saripan, M. I., and Mashohor, S. (2010). Review of brain mri image segmentation methods. *Artificial Intelligence Review*, 33(3):261–274.

Brain, A. M. (2013). Brain web: 20 anatomical models of 20 normal brains, available at. http://brainweb.bic.mni.mcgill.ca/brainweb/anatomic_normal_20.html.

Caselles, V., Kimmel, R., and Sapiro, G. (1997). Geodesic active contours. *International Journal of Computer Vision*, 22(1):61–79.

Chan, T. F. and Vese, L. A. (2001). Active contours without edges. *IEEE Transactions on Image processing*, 10(2):266–277.

Elnakib, A., Gimelfarb, G., Suri, J. S., and El-Baz, A. (2011). Medical image segmentation: A brief survey. In *Multi Modality State-of-the-Art Medical Image Segmentation and Registration Methodologies*, pages 1–39. Springer.

Kass, M., Witkin, A., and Terzopoulos, D. (1988). Snakes: Active contour models. *International Journal of Computer Vision*, 1(4):321–331.

Li, C., Kao, C.-Y., Gore, J. C., and Ding, Z. (2007). Implicit active contours driven by local binary fitting energy. In *IEEE Conference on Computer Vision and Pattern Recognition, CVPR'07.*, pages 1–7. IEEE.

Li, C., Kao, C.-Y., Gore, J. C., and Ding, Z. (2008). Minimization of region-scalable fitting energy for image segmentation. *IEEE Transactions on Image Processing*, 17(10):1940–1949.

Li, C., Xu, C., Gui, C., and Fox, M. D. (2005). Level set evolution without re-initialization: a new variational formulation. In *IEEE Conference on Computer Vision and Pattern Recognition, CVPR'05.*, pages 430–436. IEEE.

Mumford, D. and Shah, J. (1989). Optimal approximations by piecewise smooth functions and associated variational problems. *Communications on Pure and Applied Mathematics*, 42(5):577–685.

Vese, L. A. and Chan, T. F. (2002). A multiphase level set framework for image segmentation using the mumford and shah model. *International Journal of Computer Vision*, 50(3):271–293.

Yang, Y., Li, C., Kao, C.-Y., and Osher, S. (2010). Split bregman method for minimization of region-scalable fitting energy for image segmentation. In *Advances in Visual Computing*, pages 117–128. Springer.

Zhang, K., Song, H., and Zhang, L. (2010). Active contours driven by local image fitting energy. *Pattern Recognition*, 43(4):1199–1206.

Zhang, Y., Matuszewski, B. J., Shark, L.-K., and Moore, C. J. (2007). A novel medical image segmentation method using dynamic programming. In *International Conference on Medical Information Visualisation-BioMedical Visualisation, MediVis'07.*, pages 69–74. IEEE.